A self-consistent analysis of temperature-dependent field-effect measurements in hydrogenated amorphous silicon thin-film transistors

Schropp, R. E. I.; Snijder, J.; Verwey, J. F.

Published in:
Journal of Applied Physics

DOI:
10.1063/1.337407

Publication date:
1986

A self-consistent analysis of temperature-dependent field-effect measurements in hydrogenated amorphous silicon thin-film transistors

R. E. I. Schropp, J. Snijder, and J. F. Verwey

Citation: Journal of Applied Physics **60**, 643 (1986); doi: 10.1063/1.337407
View online: https://doi.org/10.1063/1.337407
View Table of Contents: http://aip.scitation.org/toc/jap/60/2
Published by the American Institute of Physics

A self-consistent analysis of temperature-dependent field-effect measurements in hydrogenated amorphous silicon thin-film transistors

R. E. I. Schropp, J. Snijder, and J. F. Verwey
Department of Applied Physics, Groningen State University, Nijenborgh 18, 9747 AG Groningen, The Netherlands

(Received 4 December 1985; accepted for publication 21 March 1986)

We calculated a more accurate density of states (DOS) profile from field-effect (FE) measurements in hydrogenated amorphous silicon thin-film transistors, taking into account the anomalously changing conductivity prefactor in accordance with the Meyer–Neldel (MN) rule. We present a self-consistent analysis of the density of gap states profile, where the MN rule is, for the first time, properly considered in relation to the nonuniform shift of the Fermi level as induced by the field effect. Moreover, the calculation yields the correct flat-band voltage and the corresponding flat-band activation energy. The determination of conductivity activation energies free from any initial band bending effects is of importance in all types of transport measurements.

I. INTRODUCTION

In the past few years, much attention has been focused on hydrogenated amorphous silicon (*a*-Si:H) thin-film transistors (TFTs). These transistors can, in the near future, be used in commercially available large-area liquid crystal display (LCD) panels[1–3] and in addressable image sensors.[4,5] The characteristics of these devices are highly determined by the density of localized gap states.

Several methods have been proposed to determine the density of states (DOS) distribution using the TFT structure, such as field-effect (FE) measurements.[6–12] Moreover, in these structures other fundamental properties of *a*-Si:H can be studied by the combined effect of an applied field and illumination (photofield effect[13–15]) or by the temperature dependence of the FE.

However, these measurements and other types of transport measurements with a coplanar configuration of electrodes, including transient current techniques as well as steady-state conductivity measurements such as those of Hall effect and thermopower, may strongly be influenced by initial space-charge accumulation layers. These can be caused by (i) fixed charges at the substrate–amorphous silicon interface or in the gate insulator[16–18] and by (ii) different adsorbates or insulating overlayers at the top surface.[19–22] Especially, the question of whether the Staebler–Wronski (SW) effect[23,24] is a bulk or surface effect cannot be answered before surface effects are taken into account or preferably eliminated.

In field-effect structures with a staggered electrode configuration, some of these interface effects can be accounted for by applying a nonzero gate voltage V_g, which is called the flat-band voltage V_{FB}. Thus, by controlling the band bending by means of an applied field, interface effects at the substrate–*a*-Si:H interface can be eliminated. In many cases[6,25,26] however, V_{FB}, which has a strong effect on the results of the calculation of the DOS,[27] is arbitrarily chosen. The nonacquaintance with the exact value of V_{FB} can also lead to a wrong interpretation of other physical bulk parameters, such as the conductivity activation energy.

Another problem that should not be overlooked in the analysis of conductance measurements is the anomalously large conductance prefactor and the exponential decrease of the prefactor with decreasing conductance activation energy. The relation between the conductance prefactor and the activation energy can, over a broad range of activation energies, be described by a characteristic slope A and is known as the Meyer–Neldel (MN) rule.[28] The MN relation has been observed in all kinds of inhomogeneous materials and is generally regarded as an intrinsic property. Therefore it has been argued that it should be taken into account in any model for the transport in *a*-Si:H.[29]

In this paper, we present measurements of the FE in *a*-Si:H TFTs as a function of ambient temperature. These measurements are appropriate for study of the temperature dependence of the dc conductivity as a function of the effective Fermi level in a highly controllable manner, because there are no limitations due to impurity-related defects that are normally introduced when the Fermi level is varied by doping.[30–32]

By theoretical analysis we are able to determine the flat-band voltage in our TFTs. At the same time, the real flat-band bulk activation energy is found, the physical parameter that is of great importance to the interpretation of all kinds of transport results. Moreover, we will show that the FE strictly obeys the MN rule. In the present FE analysis, the MN rule is, for the first time, fully taken into account. The value of the MN parameter A that is applied in the calculation, is shown to have a large effect on the outcome of the DOS profiles. Therefore, we believe that conventional analysis of the FE[9–12] is fundamentally incorrect. Special care is taken to use the correct value of A and the resultant DOS distribution of undoped amorphous silicon is presented.

Accurate separation of interface and bulk effects may lead to disclosure of the origins of the MN rule and the SW effect.

II. EXPERIMENTAL DETAILS

The measurements were performed on field-effect structures as shown in Fig. 1. The gate insulator, 110 nm thick, was made by thermal oxidation at 1000 °C of an n^+-(100) single-crystal silicon wafer. An *a*-Si:H layer was deposited by decomposition of silane in a capacitively coupled glow-

 0021-8979/86/140643-07$02.40

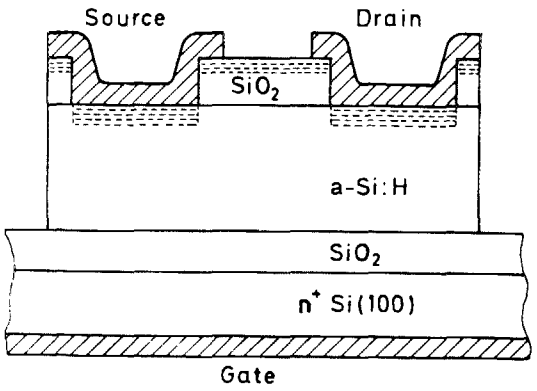

FIG. 1. Schematic cross section of the *a*-Si:H TFT as used for the FE measurements (not to scale). Regions implanted with P are horizontally striped. Hatched areas indicate the Al metallization.

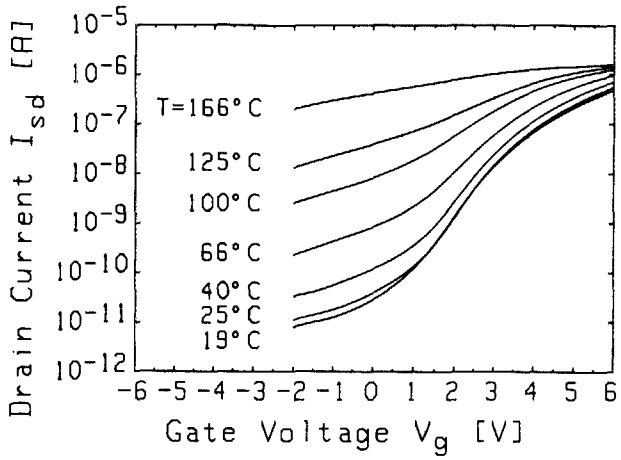

FIG. 2. Transfer characteristics (source-drain current I_{sd} vs gate voltage V_g characteristics) at various temperatures.

discharge system, followed by depositing a plasma SiO_2 layer, under the conditions summarized in Table I. Between subsequent depositions the reactor chamber was not opened, to avoid exposure to air of the *a*-Si:H film. The purpose of the SiO_2 layer is to serve as a passivating layer, so that the top fixed charge will remain low.[33,34]

In this layer, contact holes were etched to define the geometry of source and drain contacts. Before Al metallization and delineation the samples had a shallow P^+-implantation (30 keV, 10^{16} cm^{-2}), the oxide layer thereby serving as a masking layer. The gate contact was prepared by evaporation of Al at the rear face of the wafer.

In order to optimize source and drain contacts, the samples were then treated with a post-metallization anneal (PMA) at 200 °C in wet N_2 for about 30 min. By this treatment the contacts were made blocking for holes and ohmic for electrons.[35] Furthermore, the effects of exposure to light due to the SW effect during earlier stages of the fabrication are in this way reduced to a minimum.

We measured the drain current I_{sd} versus gate voltage V_g characteristics at temperatures from room temperature up to 166 °C. The measurements were performed in the dark, so that no metastable changes due to the SW effect took place.

TABLE I. Deposition conditions.

Parameter	*a*-Si:H	SiO_2
Substrate temperature(°C)	200	200
Chamber pressure (Torr)	0.4	1
rf power density (mW/cm^2)	30	30
Flow rate SiH_4 (sccm)	60	8
Flow rate N_2O (sccm)	...	160
Growth rate (nm/s)	0.15	0.8
Layer thickness (nm)	460	320
Electrode spacing (cm)	2.0	...
Diameter electrodes (cm)	24.5	...

III. EXPERIMENTAL RESULTS

The transfer characteristics are shown in Fig. 2. The conductance modulation at room temperature is almost five decades with applied gate voltage, but is, as expected, decreasing with increasing temperature. This feature is very unfavorable from an application point of view. The on/off current ratio decreases with increasing ambient temperature, as can most easily be seen from Fig. 3, where the FE current at elevated temperatures divided by the corresponding room-temperature currents is plotted. It must be noted that this plot has very much the same features as an equivalent plot of the photofield-effect current divided by the FE current in the dark.[15]

From these measurements we infer the sheet conductance $G_{sd} = I_{sd}L/V_{sd}W$ at each value of V_g, T. From the temperature dependence of the dc conductance, it follows that there is a simply activated band conduction mechanism above room temperature. At lower temperatures there seems to be a $T^{-1/4}$ behavior (not shown here), which is indicative of conduction by variable range hopping in localized gap

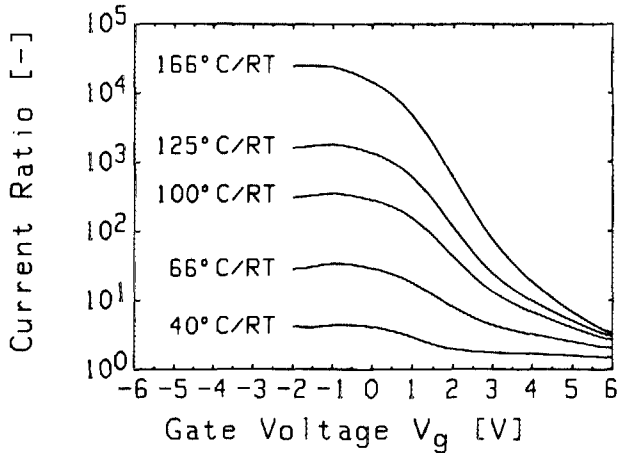

FIG. 3. Field-effect currents at various temperatures relative to corresponding room-temperature (RT) currents as a function of the gate voltage, showing the loss of switching performance.

states.[36] The activation energy E_a is determined at selected V_g values from Arrhenius plots of log G vs $1000/T$ (Fig. 4). The activation energy is effectively a function of V_g, because of different band bending conditions at increasing values of V_g. This is shown by the open dots in Fig. 5. The dependence of the conductance prefactor G_0 on the gate voltage V_g is shown in Fig. 6. This plot has very much the same features as the E_a vs V_g plot of Fig. 5.

Indeed, the FE obeys the MN rule as shown in Fig. 7. As can be seen, the points lie on a straight line with small scatter. As shown by a linear least-squares approximation, the conductance prefactor G_0 can be written as

$$G_0(V_g) = G_{00} \exp[A_{app} E_a(V_g)] , \quad (1)$$

where the apparently observed MN parameter A_{app} amounts to 23.9 eV^{-1}.

The value of A_{app} is not the same as that of the intrinsic MN parameter A, because by applying a gate voltage the shift of the Fermi level is not uniform over the bulk of the material. As shall be shown in Sec. IV B, $A_{app} > A$, because the effective thickness of the channel is generally smaller than the sample thickness and decreasing with a decrease of the effective activation energy, so that the variation of the prefactor G_0 is not as fast as is suggested by the variation of the source-drain conductance G_{sd}.

IV. METHOD OF ANALYSIS

A. The density of states profile

The theoretical outline of the FE analysis starts with the expression for the source-drain conductance G_{sd} as a function of the gate voltage V_g, assuming electron conduction only. This is given by

$$G_{sd}(V_g) = \frac{1}{d_{Si}} \int_0^{d_{Si}} G_0(x) \exp[-\beta E_a(x)] dx , \quad (2)$$

where d_{Si} is the thickness of the active layer and $\beta = 1/kT$ with k = Boltzmann's constant. The distance measured from the insulator–a-Si:H interface is denoted by x. The energy separation between the conduction-band edge and the Fermi level appearing in the Boltzmann factor is given by

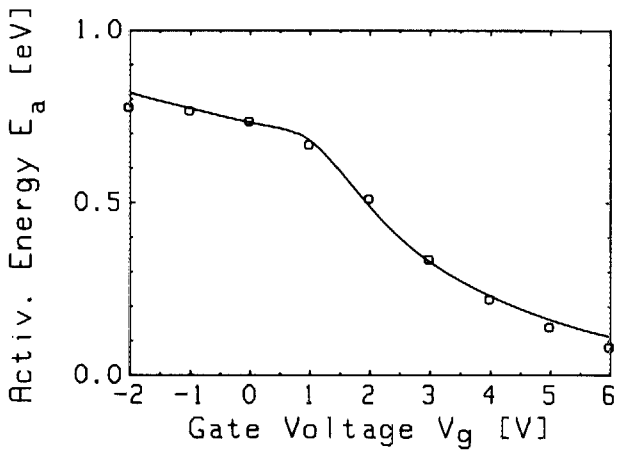

FIG. 5. Plot of the effective activation energy E_a vs applied gate voltage V_g. The open dots (O) are experimental points and the full curve is a calculated fit.

$E_a(x) = E_{aFB} - V(x)$, where E_{aFB} is the conductivity activation energy at flat bands and $V(x)$ is the electrostatic potential or band-bending parameter at a distance x, measured in eV.

Due to the band bending the prefactor $G_0(x)$ is, according to the MN rule, expressed by

$$G_0(x) = G_{00} \exp[A E_a(x)] , \quad (3)$$

where the empirically observed MN parameter A can be regarded as a constant over a broad range of activation energies, this range being generally between 0.2 and 0.7 eV for undoped material. Combining Eqs. (2) and (3) the FE conductance can be written as

$$G_{sd}(V_g) = \frac{G_{FB}}{d_{Si}} \int_0^{d_{Si}} \exp[(\beta - A) V(x)] dx , \quad (4)$$

where $G_{FB} = G_{sd}(V_{FB}) = G_{0FB} \exp(-\beta E_{aFB})$ is the drain-source conductance at flat bands.

The difference between this expression and the commonly used (Refs. 9–12) expression for the FE conductance is that β has now been replaced by $\beta - A$.

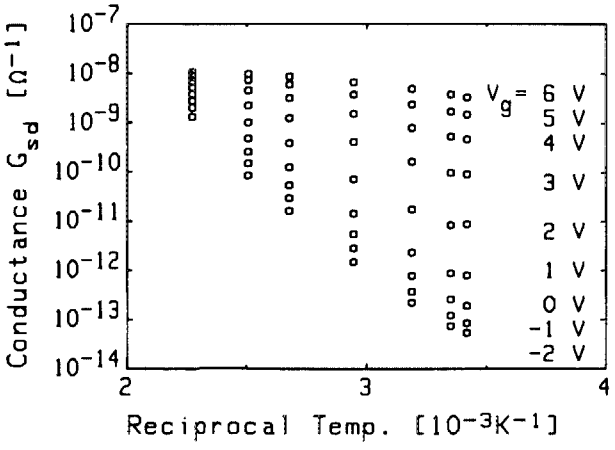

FIG. 4. Temperature dependence of the dc dark sheet conductance at various applied gate voltages.

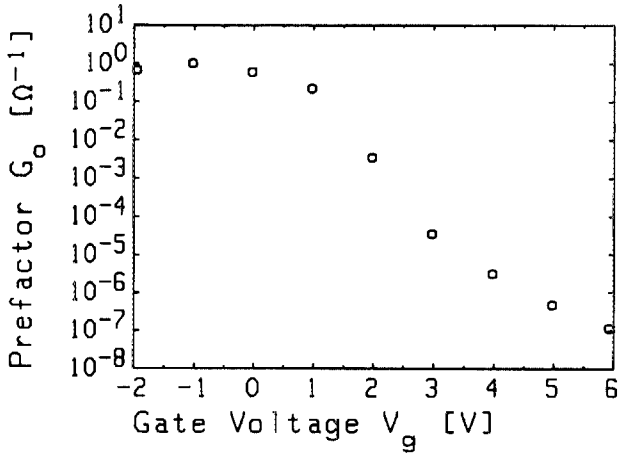

FIG. 6. Plot of the conductance prefactor G_0 vs gate voltage V_g.

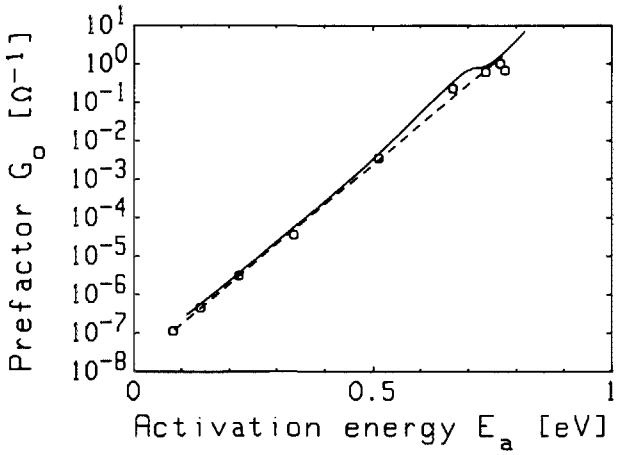

FIG. 7. Dependence of the conductance prefactor G_0 on the effective activation energy E_a, showing the Meyer–Neldel relation. The dashed line is obtained by a simple least-squares approximation to the experimental points (○), yielding $A_{app} = 23.9\,eV^{-1}$. The full line is found by calculating the G_0, E_a dependence from Eqs. (16) and (17) using $A = 18.8\,eV^{-1}$, and appropriate V_{FB} and E_{aFB} values.

The Poisson equation for the potential distribution inside the semiconductor is given by

$$\frac{d^2V(x)}{dx^2} = \frac{en[V(x)]}{\epsilon_{Si}\epsilon_0}, \tag{5}$$

with boundary conditions

$$\frac{dV(x)}{dx} = V(x) \to 0 \quad \text{if} \quad x \to d_{Si} \tag{6}$$

and

$$\left.\frac{dV(x)}{dx}\right|_{x=0} = e\frac{\epsilon_{ins}}{\epsilon_{Si}}\frac{V_F}{d_{ins}}, \tag{7}$$

where e is the electronic charge, $n[V(x)]$ is the excess density of localized charge, ϵ_0 the permittivity of free space, ϵ_{Si} the relative dielectric constant of the semiconductor, d_{ins} the thickness of the gate insulator, and $V_F = V_g - V_{FB}$. By performing a manipulation of Poisson's equation, by which the band-bending parameter V becomes the independent variable[9–11] and by applying the boundary conditions of Eqs. (6) and (7), the FE conductance is given by

$$G_{sd}(V_g) = G_{FB} + \frac{G_{FB}}{d_{Si}}\left(\frac{\epsilon_0\epsilon_{Si}}{e}\right)^{1/2} \times \int_0^{V_0(V_F)} \frac{\exp[(\beta - A)V] - 1}{\sqrt{2F(V)}}\,dV, \tag{8}$$

where $V_0 = V(0)$ is the band bending at the interface, and

$$F(V) = \int_0^V n(V')dV'. \tag{9}$$

From now on we essentially follow the derivation of Grünewald, Thomas, and Würtz.[27] It can thus be shown, that the interface band bending is related to experimentally obtained data by

$$\exp(\beta - A)V_0 - (\beta - A)V_0 - 1 = \frac{\beta - A}{G_{FB}}\frac{d_{Si}}{d_{ins}}\frac{\epsilon_{ins}}{\epsilon_{Si}} \times \left(V_F G_{sd}(V_F) - \int_0^{V_F} G_{sd}(V'_F)dV'_F\right). \tag{10}$$

The charge density is obtained from

$$n(V_0) = \frac{\epsilon_0\epsilon_{ins}}{ed_{ins}d_{Si}}\frac{G_{FB}\{\exp[(\beta - A)V_0] - 1\}}{[dG_{sd}(V_F)/dV_F]}. \tag{11}$$

The field-effect DOS function is obtained from

$$N(E) = \left|\frac{dn(V_0)}{dV_0}\right|_{V_0 = E}. \tag{12}$$

Here, we assume that all the charge goes into the localized gap states and that 0-K Fermi statistics are applicable for the occupancy of these states.

There are several reasons for the use of 0-K statistics. First of all, it is questionable whether the fine structure in $N(E)$, that can be obtained by accurate deconvolution of $n(V_0)$ with the Fermi–Dirac distribution function is relevant in a sense that it is unique to the observed FE data.[10] Second, $N(E)$ can with Eq. (12) easily be calculated by differentiation.

It can be shown that the use of 0-K statistics is justified, provided that

$$\frac{1}{N(E)}\frac{dN(E)}{dE} < \beta \tag{13}$$

holds for the density of gap states $N(E)$. As it has often been suggested that $N(E)$ exhibits an exponential distribution with a characteristic temperature of about 1000 K around midgap,[37] the requirement of Eq. (13) is considered to be fulfilled for that part of the distribution. For the remaining part, the requirement can be checked by observing the calculated $N(E)$ profile. A further justification for the use of zero-temperature statistics mixed with Boltzmann electron conduction is the excellent agreement between the activation energies calculated with this model and the experimental results (see Sec. IV B).

The calculation of $N(E)$ starts with computing $V_0(V_F)$ from Eq. (10) and $n(V_0)$ from Eq. (11) by a numerical procedure from the experimental data. In the calculations the MN parameter A and the flat-band voltage turn out to have a large effect on the resultant density of states.

In Fig. 8 we have calculated the DOS distribution for the presently considered sample using $V_{FB} = 0.8$ V and for several values of the MN parameter A. A method to obtain the correct V_{FB} is expounded in Sec. IV B. For the moment, we want to put emphasis on the effect of the value of A on the resultant DOS profile. It is clearly seen from Fig. 8, that by conventional analysis using $A = 0$ the DOS is greatly overestimated. Applying a nonzero value of A leads to a "stretch out" of the DOS profile and $N(E)$ is thus obtained over a broader range of band-gap energies. This is in contrast to other published distributions,[7,27] where $N(E)$ rises too steeply when going from the Fermi level to the conduction-band edge, so that $N(E)$ is obtained only over a small energy

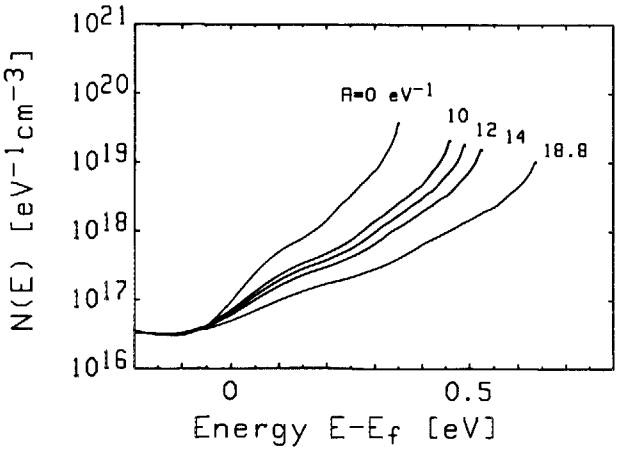

FIG. 8. The density of states function obtained from RT FE data, using various values for the MN parameter A, as indicated.

range, typically reaching no further than 0.4–0.5 eV from the Fermi level towards the upper part of the band gap.

B. Determination of the flat-band voltage and the Meyer–Neldel parameter

With a theoretical approach it is possible to calculate values of E_a as a function of V_g. If the conductivity is due to electrons excited beyond the mobility edge into the extended states, the effective activation energy can be written as

$$E_a(V_g) = -\frac{1}{G_{sd}(V_g)}\frac{dG_{sd}(V_g)}{d\beta}, \tag{14}$$

where $G_{sd}(V_g)$ is given by Eq. (8).

Differentiation of G_{sd} with respect to β yields

$$\frac{dG_{sd}(V_g)}{d\beta} = \frac{G_{sd}(V_g)}{G_{FB}}\frac{dG_{FB}}{d\beta} + \frac{G_{FB}}{d_{Si}}\left(\frac{\epsilon_0\epsilon_{Si}}{e}\right)^{1/2} \times \int_0^{V_0(V_F)} \frac{V\exp[(\beta - A)V]}{\sqrt{2F(V)}}\,dV, \tag{15}$$

where we assumed $n(V)$ independent of β, meaning that at any temperature all the charge goes into the localized states. We further assumed in Eq. (15), that the shift of the Fermi level with temperature at the interface and in the bulk is equal to zero. As for the bulk of the sample, the Fermi level is approximately at midgap so that we can neglect the statistical shift of E_F.[38] At the interface a slight relaxation of the band bending possibly takes place and a linear shift with temperature T is to be expected. However, the coefficient of this temperature shift is negligibly small (10^{-4} eV/K; Ref. 39) and can be neglected in the scope of this analysis.

Noticing that the activation energy at flat bands is given by $E_{aFB} = -(dG_{FB}/d\beta)/G_{FB}$, we obtain from Eq. (15)

$$E_a(V_g) = E_{aFB} - \frac{G_{FB}}{G_{sd}(V_g)d_{Si}}\left(\frac{\epsilon_0\epsilon_{Si}}{e}\right)^{1/2} \times \int_0^{V_0(V_F)} \frac{V\exp[(\beta - A)V]}{\sqrt{2F(V)}}\,dV. \tag{16}$$

The activation energy E_a can now be computed as a function of $V_g = V_F + V_{FB}$ from experimental room-temperature FE data at any desired value of V_{FB} and A. The correct values for V_{FB} and A are uniquely obtained by fitting the calculated curves to a set of experimentally determined $E_a(V_g)$ values with a least-squares routine. The flat-band voltage as well as the MN parameter have an effect on the shape of the theoretical curve. The flat-band activation energy E_{aFB} is simply found by interpolation at V_{FB} from experimental $E_a(V_g)$ data. The only effect of a change in E_{aFB} is a rigid displacement of the curve along the y axis. In order to check the calculated parameters, the prefactor G_0 that would have been observed is recalculated as a function of E_a using calculated $E_a(V_g)$ values and measured $G_{sd}(V_g)$ data, using the formula

$$G_0(V_g) = G_{sd}(V_g)\exp[\beta E_a(V_g)]. \tag{17}$$

The best fit of the theoretical calculations to the measured data of this FE structure is displayed by the continuous curves in Figs. 5 and 7. We obtained for the flat-band voltage $V_{FB} = 0.8$ V, for the MN parameter $A = 18.8$ eV^{-1} and for the "real" flat-band activation energy $E_{aFB} = 0.70$ eV.

V. DISCUSSION

A. The values of physical parameters

We have outlined an experimental procedure and subsequent analysis to obtain, uniquely, the flat-band voltage V_{FB}, the "real" flat-band activation energy E_{aFB} and the bulk Meyer–Neldel parameter A using a thin-film transistor. The method is applicable if V_{FB} does not change during a field-effect measurement due to charge trapping,[18] nor as a result of the measurement itself (hysteresis). This kind of instability can be avoided by measuring at not too high gate voltages and by taking care that the duration of the negative voltage is equal to that of positive voltage. A further assumption is that V_{FB} is independent of temperature.

Another procedure[11] that uses field-effect measurements as a function of the temperature, gives only the gate voltage at which the bands are flat. Our method establishes values of E_{aFB} and A, as well. These parameters are at least as important as V_{FB}, as we have shown.

Special care has to be taken that the correct value of A is used. It is incorrect to use the apparent value of A_{app} as induced by the FE.[40] The intrinsic value of A is smaller than the apparent value because the latter is dependent on the channel width carrying the FE current and therefore on the specific density of states profile. In our calculation of the DOS, self-consistency is assured in this sense.

A gate voltage-controlled determination of the effective activation energy may reveal interesting material properties of a-Si:H. For example, in Fig. 5 it appears that the activation energy saturates towards a minimum value of $E_{a,sat} = 0.09$ eV. This value of $E_{a,sat}$ can be regarded as the width of the tail states.[41] This value is lower than that obtained by shifting the Fermi level by P doping.[30–32] This difference may reflect that tail state defects are created by relatively high doping levels.[42]

Another advantage of measuring activation energies in a field-effect structure is that interface band-bending effects can essentially be separated from bulk effects. This may be

helpful in studying the problem of whether the SW effect is an interface or a bulk effect.[43]

B. Background of the MN rule

The MN rule has been reported to be applicable whenever the effective position of the Fermi level is varied, regardless of whether this position is caused uncontrollably by preparation conditions,[44–46] surface conditions,[21] doping,[47] or photoirradiation.[29] The MN rule applies also, when the Fermi level is moved without introducing extra defect states by an applied electric field, as is shown here.

Many different explanations for the MN rule have been put forward. It has been explained by (i) a shift in the mobility edge with temperature,[44] (ii) a statistical temperature shift of the Fermi level,[48] and (iii) a gradual transition between two different conduction mechanisms.[49]

As demonstrated by using the FE, the MN rule can also be ascribed completely to the presence of external band bending, and therefore it is questionable whether or not the MN rule is an intrinsic property. A similar view has also been suggested previously,[21] prompted by measurements on samples with different surface conditions. As our theoretically derived intrinsic value for the slope A is very much the same as that generally obtained by bulk doping,[47] we suggest that the MN rule is, to a large extent, intrinsic. Nevertheless, the slope of the intrinsic MN rule can significantly be modified due to band bending at external interfaces. We believe that the intrinsic value of A spreads over a much smaller range than over the reported range of 15–35 eV^{-1}.[50] We suggest an explanation of the Meyer–Neldel relation in terms of band bending at internal microscopic surfaces, originating from defects or impurities. This is confirmed by the fact that the value of A, as obtained by applying the SW effect, is influenced by the concentration of doping gas impurities.[29] It is clear that one has to be careful in comparing MN slopes of differently deposited samples, as the uncontrolled amount of interfering band bending has influence on the MN behavior.

VI. CONCLUSIONS

We have proposed a self-consistent method for the evaluation of the flat-band voltage in a-Si:H thin-film transistors, based on analysis of the FE measured at different temperatures. At the same time, the bulk activation energy and the intrinsic slope of the Meyer–Neldel relation are, by this method, determined unambiguously.

It is shown that the FE strictly obeys the Meyer–Neldel rule, but with an apparently steeper characteristic slope, indicating that this is often only partly an intrinsic property. By employing the MN parameter self-consistently, the density of states distribution has been computed and significant differences have been shown in the calculated outcome using different MN slopes. By using the correct A the FE density of states is lower than without accounting for the MN rule.

The investigation of the activation energies and the MN parameter in a FE structure can possibly lead to an answer to the question, whether the Staebler–Wronski effect has to be explained by interface or by bulk effects. Applying the reported analysis, bulk and interface effects can be measured separately.

In addition, the saturation value of E_a is interpreted as the tail-state width, which turns out to be 0.09 eV.

ACKNOWLEDGMENTS

We wish to thank S. Bakker, J. Bomer, and B. in't Veen for the preparation of the devices and M. Mulder for the implantations. We thank C. van Berkel and M. J. Powell (Philips Research Labs, Redhill) for their supplementary DOS calculations. This work was supported by the Foundation for Fundamental Research on Matter (Stichting F.O.M., Utrecht).

[1] A. J. Snell, K. D. Mackenzie, W. E. Spear, P. G. LeComber, and A. J. Hughes, Appl. Phys. **24**, 357 (1981).
[2] M. V. C. Stroomer, M. J. Powell, B. C. Easton, and J. A. Chapman, Electron. Lett. **18**, 858 (1982).
[3] Y. Okubo, T. Nakagiri, Y. Osada, M. Sugata, N. Kitahara, and K. Hatanaka, Society for Information Display International Symposium 1982, Digest of Technical Papers (1982) p. 40.
[4] M. Matsumura, H. Hayama, Y. Nara, and Y. Ishibashi, IEEE Electron Device Lett. **EDL-1**, 182 (1980).
[5] A. J. Snell, A. Doghmane, P. G. LeComber, and W. E. Spear, Appl. Phys. **A34**, 175 (1984).
[6] W. E. Spear and P. G. LeComber, J. Non-Cryst. Solids **8–10**, 727 (1972).
[7] A. Madan, P. G. LeComber, and W. E. Spear, J. Non-Cryst. Solids **20**, 239 (1976).
[8] G. W. Neudeck and A. K. Malhotra, Solid State Electron. **19**, 721 (1976).
[9] M. Grünewald, P. Thomas, and D. Würtz, Phys. Status Solidi B **100**, K139 (1980).
[10] M. J. Powell, Philos. Mag. B **43**, 93 (1981).
[11] R. L. Weisfield and D. A. Anderson, Philos. Mag. B **44**, 83 (1981).
[12] N. B. Goodman and H. Fritzsche, Philos. Mag. B **42**, 149 (1980).
[13] T. Kagawa, N. Matsumoto, and K. Kumabe, Phys. Rev. B **28**, 4570 (1983).
[14] A. O. Harm, R. E. I. Schropp, and J. F. Verwey, Philos. Mag. B **52**, 59 (1985).
[15] R. E. I. Schropp, A. O. Harm, and J. F. Verwey, Philos. Mag. B **53** (in press).
[16] I. Solomon, T. Dietl, and D. Kaplan, J. Phys. **39**, 1241 (1978).
[17] D. G. Ast, IEEE Trans. Electron Devices **ED-30**, 532 (1983).
[18] J. Vaid and H. Fritzsche, J. Appl. Phys. **55**, 440 (1984).
[19] M. Tanielian, M. Chatani, H. Fritzsche, V. Smid, and P. D. Persans, J. Non-Cryst. Solids **35** and **36**, 575 (1980).
[20] M. Tanielian, Philos. Mag. B **45**, 435 (1982).
[21] M. Yamaguchi and H. Fritzsche, J. Appl. Phys. **56**, 2303 (1984).
[22] H. Fritzsche, Solar Energy Mater. **3**, 447 (1980).
[23] D. L. Staebler and C. R. Wronski, Appl. Phys. Lett. **31**, 292 (1977).
[24] D. L. Staebler and C. R. Wronski, J. Appl. Phys. **51**, 3262 (1980).
[25] M. J. Powell, B. C. Easton, and D. H. Nicholls, J. Appl. Phys. **53**, 5068 (1982).
[26] M. Hirose, T. Suzuki, and G. H. Döhler, Appl. Phys. Lett. **34**, 234 (1979).
[27] K. Weber, M. Grünewald, W. Fuhs, and P. Thomas, Phys. Status Solidi B **110**, 133 (1982).
[28] W. Meyer and H. Neldel, Z. Tech. Phys. **18**, 588 (1937).
[29] P. Irsigler, D. Wagner, and D. J. Dunstan, J. Phys. C **16**, 6605 (1983).
[30] W. E. Spear and P. G. LeComber, Philos. Mag. **33**, 935 (1976).
[31] M. Taniguchi, M. Hirose, and Y. Osaka, J. Cryst. Growth **45**, 126 (1978).
[32] J. Magariño, D. Kaplan, A. Friederich, and A. Deneuville, Philos. Mag. B **45**, 285 (1982).
[33] M. J. Powell and J. W. Orton, Appl. Phys. Lett. **45**, 171 (1984).
[34] S. Kawai, N. Takagi, T. Kodana, K. Asama, and S. Yangisawa, Society for Information Display International Symposium 1982, Digest of Technical Papers (1982), p. 42.
[35] R. E. I Schropp, J. W. C. Veltkamp, J. Snijder, and J. F. Verwey, IEEE Trans. Electron Devices **ED-32**, 1757 (1985).
[36] N. F. Mott and E. A. Davis, *Electronic Processes in Non-Crystalline Materials*, 2nd ed. (Oxford, New York, 1979).
[37] M. Shur and M. Hack, J. Appl. Phys. **55**, 3831 (1984).

[38]D. I. Jones, P. G. LeComber, and W. E. Spear, Philos. Mag. B **36**, 541 (1977).
[39]R. Meaudre, Philos. Mag. B **51**, L57 (1985).
[40]J. Jang and C. Lee, J. Non-Cryst. Solids **59** and **60**, 281 (1983).
[41]K. D. Mackenzie, A. J. Snell, I. French, P. G. LeComber, and W. E. Spear, Appl. Phys. A **31**, 87 (1983).
[42]W. Zhong-Yan and S. Yue-hua, Solar Energy Mater. **11**, 273 (1984).
[43]D. J. Dunstan (private communication).
[44]W. E. Spear, D. Allan, P. G. LeComber, and A. Ghaith, Philos. Mag. B **41**, 419 (1979).
[45]W. E. Spear, J. Non-Cryst. Solids **35** and **36**, 357 (1980).
[46]H. Fritzsche and M. Tanielian, in *Conference on Tetrahedrally Bonded Amorphous Semiconductors,* edited by R. A. Street, D. K. Biegelsen, and J. C. Knights (Carefree, Arizona, 1981), p. 318.
[47]D. E. Carlson and C. R. Wronski, in *Amorphous Semiconductors,* Topics in Applied Physics, Vol. 36, edited by M. H. Brodsky (Springer, New York, 1979), Chap. 10, p. 287.
[48]H. Overhof and W. Beyer, J. Non-Cryst. Solids **35** and **36**, 375 (1980).
[49]W. Rehm, R. Fisher, J. Stuke, and H. Wagner, Phys. Status Solidi B **79**, 539 (1977).
[50]J. Bullot, M. Galin, M. Gauthier, B. Bourdon, and Y. Catherine, J. Phys. **43**, 1419 (1982).